

Elucidating the principles of the molecular organization of heteropolymeric tight junction strands

Jörg Piontek · Susanne Fritzsche · Jimmi Cording · Sandra Richter · Jens Hartwig · Maria Walter · Dan Yu · Jerrold R. Turner · Claudia Gehring · Hans-Peter Rahn · Hartwig Wolburg · Ingolf E. Blasig

Received: 4 November 2010 / Revised: 7 March 2011 / Accepted: 24 March 2011 / Published online: 1 May 2011
© Springer Basel AG 2011

Abstract Paracellular barrier properties of tissues are mainly determined by the composition of claudin heteropolymers. To analyze the molecular organization of tight junctions (TJ), we investigated the ability of claudins (Cld) to form homo- and heteromers. Cld1, -2, -3, -5, and -12 expressed in cerebral barriers were investigated. TJ-strands were reconstituted by claudin-transfection of HEK293-cells. *cis*-Interactions and/or spatial proximity were analyzed by fluorescence resonance energy transfer inside and outside of strands and ranked: Cld5/Cld5 > Cld5/Cld1 > Cld3/Cld1 > Cld3/Cld3 > Cld3/Cld5, no Cld3/Cld2. Classic Cld1, -3, and -5 but not non-classic Cld12 showed homophilic *trans*-interaction. Freeze-fracture electron microscopy revealed that, in contrast to classic claudins, YFP-tagged Cld12 does not form homopolymers. Heterophilic *trans*-interactions were analyzed in cocultures of

differently monotransfected cells. *trans*-Interaction of Cld3/Cld5 was less pronounced than that of Cld3/Cld1, Cld5/Cld1, Cld5/Cld5 or Cld3/Cld3. The barrier function of reconstituted TJ-strands was demonstrated by a novel imaging assay. A model of the molecular organization of TJ was generated.

Keywords Claudins · FRET · Protein–protein interaction · Tight junction

Introduction

Tight junctions (TJ) form a paracellular barrier in epithelia and endothelia. They regulate and limit the paracellular permeation of ions, solutes, and proteins [1]. TJ appear as fusions of the membranes of two neighboring cells (transmission electron microscopy) and as an anastomosing network of strands composed of transmembrane proteins (freeze-fracture electron microscopy) [2]. The tetraspan membrane proteins of the claudin (Cld) family constitute the backbone of TJ by *trans*- (head to head) and *cis*- (side by side) interactions [3, 4]. The various claudin subtypes exhibit tissue-specific expression patterns and differ in their barrier properties [5]. For instance, Cld5 tightens the blood–brain barrier against small molecules up to 800 Da [6]; Cld2 forms paracellular pores for monovalent cations; and a complex between Cld16 and Cld19 creates pores for divalent cations [7, 8]. Residues in the first extracellular loop (ECL1) of claudins determine the ability to form paracellular ion pores as well as their charge selectivity [5, 9]. In addition, Gln44 in the ECL1 of human Cld3 prevents heterophilic *trans*-interactions with Cld4 [10]. Involvement of the ECL2 in *trans*-interaction between Cld5 molecules of adjacent cells during formation of TJ strands and

Electronic supplementary material The online version of this article (doi:10.1007/s00018-011-0680-z) contains supplementary material, which is available to authorized users.

J. Piontek (✉) · S. Fritzsche · J. Cording · S. Richter · M. Walter · C. Gehring · I. E. Blasig
Leibniz-Institut für Molekulare Pharmakologie,
Robert-Rössle-Str. 10, 13125 Berlin, Germany
e-mail: piontek@fmp-berlin.de

J. Hartwig · H.-P. Rahn
Max-Delbrück-Center for Molecular Medicine, Berlin, Germany

D. Yu · J. R. Turner
Department of Pathology, The University of Chicago,
Chicago, IL 60637, USA

H. Wolburg
Institute of Pathology, University Hospital Tübingen,
Tübingen, Germany

paracellular barrier development has been demonstrated in vitro [3, 11] and in vivo [12].

Claudins can functionally be divided into barrier-forming, e.g., Cld1, -3, -4, -5, and pore-forming claudins, e.g., Cld2, -7, -10, -16, [5]. Based on sequence homology studies, claudins can be grouped as classic claudins (Cld1–10, -14, -15, -17, -19) with high homology within this group and non-classic claudins (Cld11, -12, -13, -16, -18, -20 to -24) with lower homology [5]. In line with the sequence homology, the classic claudins are likely to share a common helix-turn-helix structure of the ECL2 that is involved in paracellular tightening [3, 11].

Most epithelial and endothelial cells express an assortment of different claudins and it is assumed that they form heteropolymers [13]. However, the pattern of heterophilic compatibility of claudin subtypes is incomplete and the underlying molecular mechanisms are not known. The morphology of TJ-strands in a given tissue depends on the claudin composition [14]. Most epithelia contain continuous strands with intramembranous particles associated with the protoplasmic face (P-face) of the plasma membrane. The very leaky and often fenestrated endothelia of peripheral blood vessels contain discontinuous strands, associated with the exoplasmic face (E-face). In contrast, the very tight brain capillary endothelial cells contain TJ-strands with particles on the P- and E-face [15]. Transfection experiments show that Cld1 and Cld3 form P-face-associated continuous strands where as Cld2, -5, -6, -11 form discontinuous strands partly or fully associated with the E-face. Coexpression of Cld2 with Cld1 or Cld3 increases P-face association and strand continuity [13]. Coexpression of Cld5 with Cld3 correlates with high P-face association and tightness of brain endothelial cells [16, 17]. In summary, freeze fracture and functional data suggest that the combination and stoichiometry of claudin subtypes in heteropolymeric strands defines their P/E-face association and continuity as critical determinants of TJ barrier function.

In this study, homo- and heterophilic interactions between claudins assumed to be expressed in cerebral barriers (Cld1, -2, -3, -5, and -12; [6, 14]) were systematically investigated. The data improve the understanding of the oligomerization of TJ proteins.

Materials and methods

Cell culture, transfection

HEK293 cells (HEK cells) were maintained in Dulbecco's modified Eagle's medium (DMEM, Invitrogen) supplemented with 10% fetal calf serum, 100 units/ml penicillin, 100 µg/ml streptomycin and 1% L-alanyl-L-glutamine

(Invitrogen). Transient transfections of HEK cells were performed with Lipofectamine 2000 according to the supplier's recommendations (Invitrogen). Stable lines were selected by 0.5 or 1 mg/ml G418 (Calbiochem). To avoid the development of clonal variations, pools containing different Cld5-YFP-expressing and non-expressing colonies were used. In addition, cells were sorted with FACS Vantage SE System (BD Biosciences) to achieve cultures in which >95% of the cells express the CFP/YFP-construct.

Mammalian expression vectors and site-directed mutagenesis

Expression vectors for claudins were based on pECFP-N1/pEYFP-N1 (Clontech). Plasmids encoding mouse Cld5_{wt}-CFP, Cld5_{wt}-YFP, mutants thereof and corticotropin releasing factor receptor1 (CRFR1)-YFP [3], plasmids encoding mouse Cld3L_{wt}-CFP, Cld3L_{wt}-YFP, Cld5_{wt}, Cld3_{wt}, Cld3_{Y147A} [18] and CFP-YFP tandem construct [19] have been described previously. Plasmids encoding Cld3-CFP or Cld3-YFP were generated by amplifying full-length Cld3 and introduction of SalI and BamHI restriction sites before and after the coding sequence by PCR from Cld3L_{wt}-YFP as template. The products were subcloned in pEYFP-N1 and pECFP-N1, respectively. A plasmid encoding rat Cld12-YFP was generated by amplifying full-length Cld12 without the stop codon and introduction of HindIII and BamHI restriction sites by PCR from template plasmid (kindly provided by Dr. T. Terasaki, Sendai, Japan). The product was subcloned in pEYFP-N1. Plasmids encoding human Cld1-YFP or Cld2-YFP were generated by amplifying full-length claudins without the stop codon by PCR from pcDNA3.11_Cld1 and pcDNA3.11_Cld2 as templates (kindly provided by Dr. M. Fromm, Berlin, Germany) and subcloned in pEYFP-N1.

Immunocytochemistry and live-cell imaging

Immunocytochemistry was performed as described [3]. For live-cell imaging, transfected cells were transferred to 1 ml DMEM, 10 mM (*N*-(2-hydroxyethyl)piperazine-*N'*-(2-ethanesulfonic acid) pH 7.5 without phenol red. The plasma membrane was visualized by addition of 20 µl trypan blue, 0.05% in phosphate buffered saline (PBS). Cells were examined with an LSM 510 META system, using an Axiovert 135 microscope equipped with a PlanNeofluar 100×/1.3 objective (Zeiss) [3]. To quantify claudin enrichment at contacts between two claudin-expressing cells, intensity profiles of confocal images of living cells were analyzed using the LSM 510 software (Zeiss). Contacts between two cells were identified by the trypan blue fluorescence peaks. For each cell pair, ≥5 fluorescence

intensity profiles were quantified. For cultures of Cld-CFP- or Cld-YFP-expressing cells the enrichment factor (E_F) was calculated as: (intensity at contact between two claudin-expressing cells)/(intensity at contact between an expressing and a non-expressing cell $\times 2$) [3]. For cocultures of Cld-CFP- and Cld-YFP-expressing cells the enrichment factor (E_F) was calculated as: (intensity at contact between a Cld-CFP- and a Cld-YFP-expressing cells)/(intensity at contact between an expressing and a non-expressing cell). $E_F > 1.5$ (E_F of control + 2 SD) was considered as enrichment. In addition, the frequency of enrichments P_E (pairs of contacts with $E_F > 1.5$) was determined. Similarly, contact enrichment in fixed and stained cultures was determined using confocal images, intensity profiles, and Axiovision software (Zeiss). Rabbit anti-Cld3 and Cy3-conjugated goat anti-mouse antibodies (Invitrogen) were used for immunocytochemistry.

For determination of the barrier function of claudins, cells were replated on poly-L-lysine-coated glass coverslips, after 2–3 days washed with Hank's buffered salt solution (HBSS) and incubated with 0.25 $\mu\text{g/ml}$ CellMask™ Deep Red plasma membrane stain (Invitrogen) in HBSS for 5 min. CFP, YFP and CellMask™ f ($\lambda_{\text{ex}} = 633$ nm, $\lambda_{\text{em}} = 650\text{--}710$ nm) was imaged within 5 min. As a measure for the diffusion barrier preventing CellMask™ labeling, the barrier ratio (B_r), was determined using fluorescence intensity profiles as: (CellMask™ intensity at contact between a construct-expressing and a non-expressing cell)/(intensity at contact between two construct-expressing cells). At least 15 pairs of contacts were analyzed for each sample.

FRET (fluorescence resonance energy transfer) analysis by confocal microscopy

Cells were cotransfected with plasmids encoding CFP- and YFP-fusion proteins of claudins or CRFR1. CRFR1-YFP was used as negative control, as this receptor was found to colocalize with Cld5 at cell–cell contacts but does not interact with Cld5 [19]. FRET acceptor photobleaching was performed 3 days after transfection as described [3]. Briefly, CFP and YFP were excited at 458 and 514 nm and detected from 463–495 and 527–634 nm, respectively. Photobleaching of YFP at the area of cell–cell contacts was performed by using 15–25 pulses of the 514-nm argon laser line at 100% intensity. For quantitation, the laser and detector settings were kept constant, and only cells with CFP and YFP intensities below saturation were used. FRET-efficiency (F_E) was calculated as $F_E = (IA - IB) \times 100/IA$, where IB and IA refer to the CFP intensity before and after photobleaching. In each experiment, the pair Cld5_{wt}-CFP/Cld5_{wt}-YFP was the internal standard. The relative F_E was calculated as the F_E of a distinct pair of

CFP/YFP- fusion proteins divided by F_E of Cld5_{wt}-CFP/Cld5_{wt}-YFP. In addition, the FRET efficiency was normalized to a YFP/CFP intensity ratio of 2 ($F_E - \text{YFP/CFP} = 2$), because the FRET efficiency was strongly dependent on the YFP/CFP intensity ratio (Fig. S1). For this, logarithmic regression was used to obtain an equation with which $F_E - \text{YFP/CFP}$ was calculated for YFP/CFP intensity ratio = 2.

FRET analysis by flow cytometry

Cells were cotransfected with plasmids encoding CFP- and YFP-fusion proteins. Two days later, single cell suspensions were prepared by gentle trypsinization, washing, resuspension in PBS containing 5 mM EDTA at 4°C and filtration through a cell strainer (35 μm) before analysis. FRET measurements were performed using a FACSAria II (BD Bioscience) equipped with 405 and 488-nm laser lines. To measure CFP and FRET, cells were excited at 405 nm and fluorescence was detected in the CFP channel with a 450/50 filter, while the FRET-signal was measured with a 525/50 filter. To detect YFP, cells were excited at 488 nm while emission was taken with a 530/30 filter. All dead cells and debris were excluded from the analysis based on forward and sideward scatter gating. To control for autofluorescence and automatic compensation non-transfected and single-transfected cells were included. 50,000 events/sample were analyzed using FlowJo (Tree-star) to identify the double-positive transfected cell population and OriginPro (OriginLab) was used to normalize the FRET and YFP values relative to the CFP intensity. A first-order exponential decay regression was performed using the equation $\{\text{FRET/CFP}\} = A1 \times \exp(-\{\text{YFP/CFP}\}/t1) + y0$ ($A1$, $t1$, $y0$ regression parameter determined by OriginPro). To take into account the dependence of the FRET-efficiency on the acceptor/donor ratio (YFP/CFP), FRET/CFP was calculated for the standardized YFP/CFP intensity ratio of 5. As a measure of the FRET-efficiency the FRET-ratio_{FC} was calculated as $(\text{FRET/CFP})_{\text{sample}} - (\text{FRET/CFP})_{\text{Cld5/CRFR1}}$. Cld5/CRFR1 served as internal negative control for unspecific FRET in each experiment.

FRET analysis by spectrofluorometry

Cell suspensions (as described above) were analyzed in a FP-6500 spectrofluorometer (JASCO). CFP-fluorescence was detected with $\lambda_{\text{excitation}} = 425 \pm 5$ nm and $\lambda_{\text{emission}} = 475 \pm 5$ nm, YFP-fluorescence with $\lambda_{\text{excitation}} = 490 \pm 5$ nm and $\lambda_{\text{emission}} = 525 \pm 5$ nm and FRET-Signal with $\lambda_{\text{excitation}} = 425 \pm 5$ nm and $\lambda_{\text{emission}} = 525 \pm 5$ nm. Crosstalk of YFP-fluorescence to the CFP- and FRET-signal was determined experimentally with sample

containing YFP or CFP, only (for $\lambda_{\text{excitation}} = 425 \pm 5$ nm and $\lambda_{\text{emission}} = 475 \pm 5$ nm the signal was 2% of the YFP-fluorescence ($\varepsilon_1 = 0.02$) and for $\lambda_{\text{emission}} = 525 \pm 5$ nm the signal was 5% of the YFP-fluorescence ($\varepsilon_2 = 0.05$). As a measure of the FRET-efficiency the FRET-ratio_S was calculated as $\text{FRET-ratio}_S = (\text{FRET-signal} - \varepsilon_2 \times \text{YFP-fluorescence}) / (\text{CFP-fluorescence} - \varepsilon_1 \times \text{YFP-fluorescence})$.

Fluorescence recovery after photobleaching

Fluorescence recovery after photobleaching (FRAP) was performed on a DM4000 microscope (Leica) equipped with a MicroPoint Laser System (Photonic Instruments), Leica 63X UVI objective, and 37°C heated stage controlled by MetaMorph 7 (MDS). A region of interest was bleached with a nanosecond laser pulse using low intensities and <1 s exposures to minimize phototoxicity. MetaMorph 7 was used for analysis, as described [20, 21].

Freeze-fracture electron microscopy

HEK cells were transfected with claudin-constructs, 3 days later, washed with PBS, fixed with 2.5% glutaraldehyde (electron microscopy grade, Sigma-Aldrich) in PBS for 2 h, washed and processed for freeze-fracture electron microscopy as reported [22].

Statistics

Unless stated otherwise, results are shown as mean \pm SEM. Statistical analyses were performed by one-way analysis of variance (ANOVA) and followed by an unpaired Student's *t* test. $p < 0.02$ was taken as significantly different.

Results

The classic claudin1, -3 and -5, but not the non-classic claudin12, are capable of homophilic *trans*-interactions

To compare the ability of the blood–brain barrier relevant Cld1, -3, -5, and -12, to form *trans*-interactions, the enrichment of claudins at contacts between HEK cells transfected with plasmids encoding Cld-YFP was analyzed using a previously established assay [3]. Marked enrichment of Cld1, -3, and -5, but not Cld12 or the negative CRFR1, was shown (Fig. 1). This indicates that the classic Cld1, -3, and -5 [5] but not the non-classic Cld12, have similar abilities for homophilic *trans*-interaction.

Determinants of *trans*-interactions in extracellular loop 2 are conserved between claudin5 and claudin3

Previously, we have shown that defined residues (e.g., Y148) in the ECL2 of murine Cld5 conserved among classic claudins [5] are involved in homophilic *trans*-interactions [3]. Therefore, we proposed that homologous residues are involved in homophilic *trans*-interaction of other classic claudins. To test this, HEK cells were transfected with murine Cld3_{wt} or Cld3_{Y147A} (corresponding to Cld5_{Y148A}) and the development of *trans*-interactions was assessed by enrichment of Cld3 at contacts between two Cld-expressing cells. In contrast to Cld3_{wt} (Fig. 2a, b), Cld3_{Y147A} (Fig. 2c, d) showed no enrichment at contacts. For Cld3_{wt} an enrichment factor (E_F) of 2.8 was determined compared to $E_F = 0.8$ for Cld3_{Y147A} (Fig. 2e). In addition, the percentage of contacts with a $E_F > 1.5$ (P_E) was for Cld3_{wt} (91%) much higher than for Cld3_{Y147A} (12%, Fig. 2f). This indicates that Y147A inhibits *trans*-interaction and, therefore, that the determinants for *trans*-interaction in the ECL2 are, at least, partially conserved between the classic claudins Cld5 and Cld3.

Heterophilic claudin3/claudin5 *trans*-interactions are weaker than claudin3/claudin1-, claudin5/claudin1-, and homophilic *trans*-interactions

In order to compare the homo- and heterophilic *trans*-interactions of Cld1, -3, and -5, mixed cocultures of HEK cells monotransfected with Cld-CFP- or Cld-YFP constructs were analyzed by confocal microscopy. Strong coenrichment was detected for Cld5-YFP/Cld5-CFP, Cld3-YFP/Cld3-CFP, Cld1-YFP/Cld5-CFP and Cld1-YFP/Cld3-CFP (Fig. 3a–l). For cocultures of Cld5-YFP/Cld3-CFP (Fig. 3m–r) coenrichment was much less prominent but still greater than for Cld5_{Y148A}-YFP/Cld3-CFP (Fig. 3s–u) that showed no contact enrichment. Quantitative analysis (Fig. 3v) indicates that homophilic Cld3- and Cld5 *trans*-interactions as well as heterophilic Cld5/Cld1- and Cld3/Cld1 *trans*-interactions can be formed to a similar extent whereas Cld3/Cld5 *trans*-interactions are much weaker. In addition, the latter is abolished by the substitution Y148A in Cld5. Despite the fact that the Cld3/Cld5 coenrichment was not prominent, Cld3-CFP-containing vesicles (Fig 3p–r, arrow heads) were detected in Cld5-YFP-expressing cells to an extent similar to Cld5-CFP-containing vesicles in Cld5-YFP-expressing cells and Cld5-YFP-containing vesicles in Cld5-CFP-expressing cells (Fig 3a–c, arrow heads). Thus claudins are, at least partly, internalized together with *trans*-interacting claudins of a neighboring cell, as reported earlier [23]. Hence, this coendocytosis indicates Cld3/Cld5 *trans*-interaction.

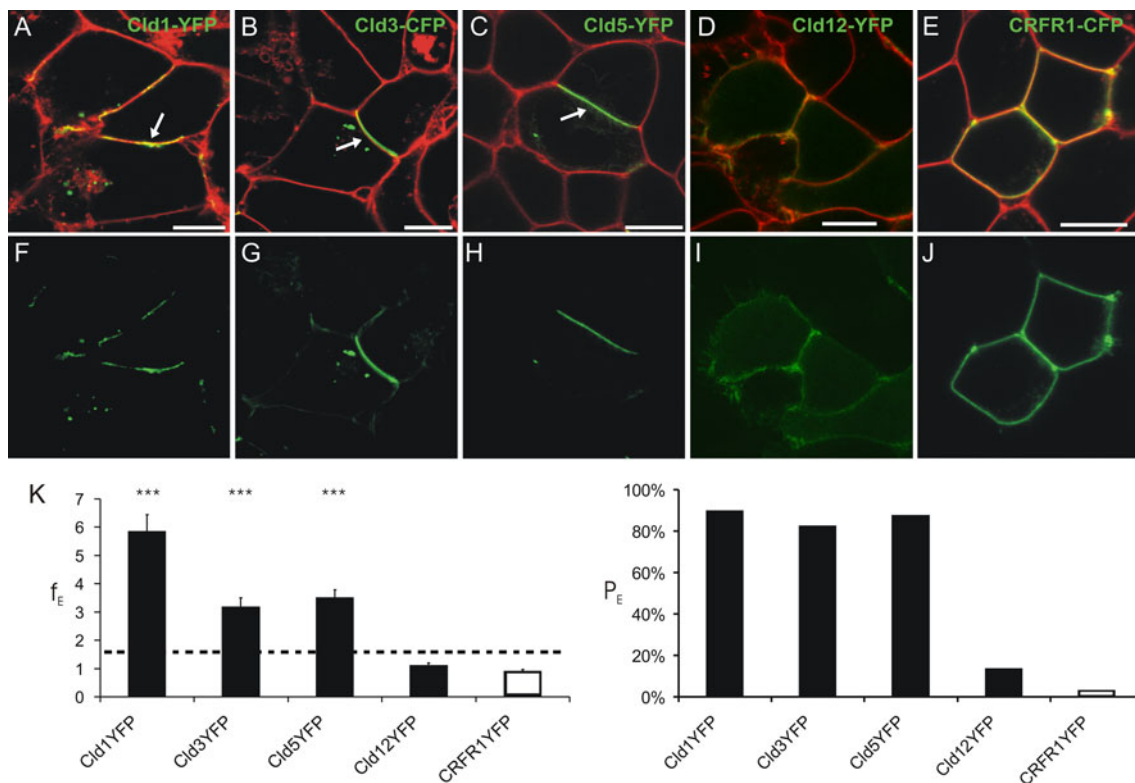


Fig. 1 Homophilic *trans*-interaction of claudin (Cld)-1, -3, and -5 but not -12. Confocal microscopy of living HEK cells stably transfected with Cld1-YFP (a, f), Cld3-CFP (b, g), Cld5-YFP (c, h), Cld12-YFP (d, i), and transiently transfected with corticotropin releasing factor receptor 1 (CRFR1)-CFP (g, j). Cld1, -3, -5 but not -12 and CRFR1 (green) are enriched (arrows) at contacts between two claudin-expressing cells indicating *trans*-interaction. Plasma membrane was

visualized with trypan blue (a–e, red). a–e, merge of CFP/YFP and trypan blue; f, h, i, YFP; g, j, CFP. Bar, 10 μ m. k Quantification of contact enrichment. For Cld1, Cld3, and Cld5, but not Cld12, the factor of contact enrichment (E_F) and the percentage of contacts with $E_F > 1.5$ (P_E) are much higher than for the negative control (CRFR1). *** $p < 0.001$ compared to CRFR1-YFP; E_F , mean + SEM; $n \geq 40$; dotted line, threshold above *trans*-interaction is considered

Coexpressed claudins colocalize only partly

The subcellular distribution of claudins was compared by transient coexpression for pairs of Cld1, -2, -3, and -5 in HEK cells and subsequent analysis by confocal microscopy (Fig. 4). Compared to stable transfection (Fig. 1), the amount of claudins in intracellular compartments was higher. Nevertheless, at contacts between transient transfectants colocalization of all claudin pairs was observed. Strong colocalization in intracellular compartments (arrow heads) was found for Cld3/Cld1 (Fig. 4b), partially for Cld5/Cld1 (Fig. 4d) but not for Cld3/Cld5 and Cld3/Cld2 (Fig. 4a, c). These differences in subcellular distribution indicate subtype-specific differences in capacity for heterophilic *cis*-interactions, targeting to the plasma membrane and/or internalization of the claudins.

Analysis of *cis*-interaction at cell–cell contacts indicates claudin subtype-specific differences

Due to the limited resolution of light microscopy apparent colocalization is not sufficient to demonstrate interaction

between claudins. Hence, fluorescence resonance energy transfer (FRET) was applied to investigate homo- and heterophilic *cis*-interactions between Cld1, -2, -3, and -5 at cell–cell contacts, HEK cells were cotransfected with respective pairs of YFP- and CFP-fusion proteins of claudins. FRET was analyzed at contacts of living cells by acceptor photobleaching [19]. The FRET-efficiency (F_E) was strongly dependent on the acceptor/donor (YFP/CFP) ratio but independent of the YFP– or YFP + CFP intensity (measure for expression level) as shown for Cld5-CFP/Cld5-YFP as an example (Fig. S1). This underlines the specificity of the FRET-signal since it indicates a clustered but not random distribution of claudins [24].

Due to the dependence on YFP/CFP ratios, the F_E of different claudin pairs was compared for cells with similar YFP/CFP ratio (Fig. 5, black columns). In addition, the F_E was normalized to a YFP/CFP fluorescence intensity ratio of 2 (Fig. 5, gray columns). As shown previously [3], the mean F_E for Cld5-CFP/Cld5-YFP was ten times higher than for that of the negative control, Cld5/CRFR1. The normalized F_E decreased in the order: Cld5/Cld5, Cld5/Cld1, Cld3/Cld1 > Cld3/Cld3 > Cld3/Cld5. For these, but

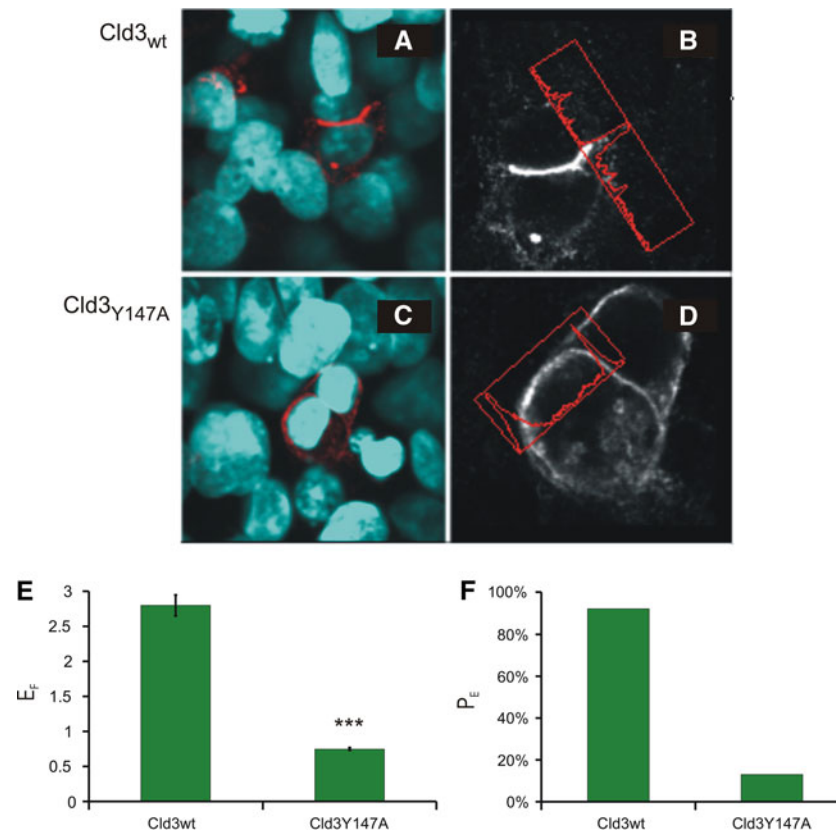


Fig. 2 Determinant for *trans*-interaction in the extracellular loop2 (ECL2) is conserved between Cld5 and Cld3. Three days after transfection of HEK cells with Cld3_{wt} (a, b) or Cld3_{Y147A} (c, d) cells were fixed, stained against Cld3 (red in a, c; white in b, d) and nuclei (blue in a, c) and enrichment at cell–cell contacts quantified using fluorescence intensity profiles (b, d; red box). The factor of contact

enrichment (E_F) was four times and the percentage of contacts showing an enrichment (P_E) 6.5 times higher for Cld3_{wt} than for Cld3_{Y147A} (e, f). This indicates that the substitution Y147A inhibits *trans*-interaction of Cld3. Mean \pm SEM; $n = 123$ for Cld3_{wt}, $n = 213$ for Cld3_{Y147A}; *** $p < 0.001$, compared to Cld3_{wt}

not for Cld3/Cld2, F_E were significantly higher than for the negative control. For Cld3, fusion constructs without and with a flexible linker between Cld3 and CFP/YFP (Cld3L) produced similar results (Fig 5.). This indicates that the lower F_E for Cld3/Cld3 and Cld3/Cld5 compared to Cld5/Cld5 are not due to sterical hindrance of the CFP/YFP-tag in Cld3-containing strands. In addition, Cld3-CFP/Cld5-YFP and Cld3-YFP/Cld5-CFP gave similar results. In summary, these data indicate claudin subtype-specific differences in *cis*-interaction at cell–cell contacts. The absence of FRET between Cld3-CFP and Cld5_{Y148A}-YFP further suggests that the *trans*-interaction (that is inhibited by the substitution Y148A [3]) is necessary for close proximity between Cld3 and Cld5 at cell–cell contacts.

cis-Interactions between claudins differ in a subtype-specific manner outside of cell–cell contacts

To investigate the *cis*-interaction of claudins outside of cell–cell contacts FRET was analyzed in cell suspensions by flow cytometry. This technique was applied because

thousands of cells of one sample can be analyzed individually. Previous studies have demonstrated the feasibility of detecting FRET by flow cytometry [25, 26]. However, published methods do not consider the dependence of the FRET-efficiency on the acceptor/donor ratio, YFP/CFP (see Fig. S1 and [27, 28]). Hence, we improved the analysis of the flow cytometry data by calculating, as a measure of the FRET-efficiency, the FRET-ratio_{FC} for a standardized YFP/CFP-ratio (see methods and Fig. S2).

For cells expressing different claudin-pairs, the FRET-efficiency decreased in the order: Cld5/Cld5 > Cld5/Cld1 > Cld3/Cld3 > Cld3/Cld5 (Fig. 6a). The FRET-ratio for Cld3/Cld2 was in the range of the negative control (Cld5/CRFR1). Similar results were obtained by FRET analysis of cell suspensions using spectrofluorometry (Fig. 6b), and of intracellular compartments using confocal microscopy (Fig. S3). In addition, Cld5/Cld5_{Y148A} showed a FRET-ratio similar to that of Cld5/Cld5 and Cld3/Cld5_{Y148A} showed a FRET-ratio similar to that of Cld3-Cld5 (Fig. 6a). Taken together, the data suggest that *cis*-interactions of claudins outside of cell–cell contacts differ in a subtype-specific manner.

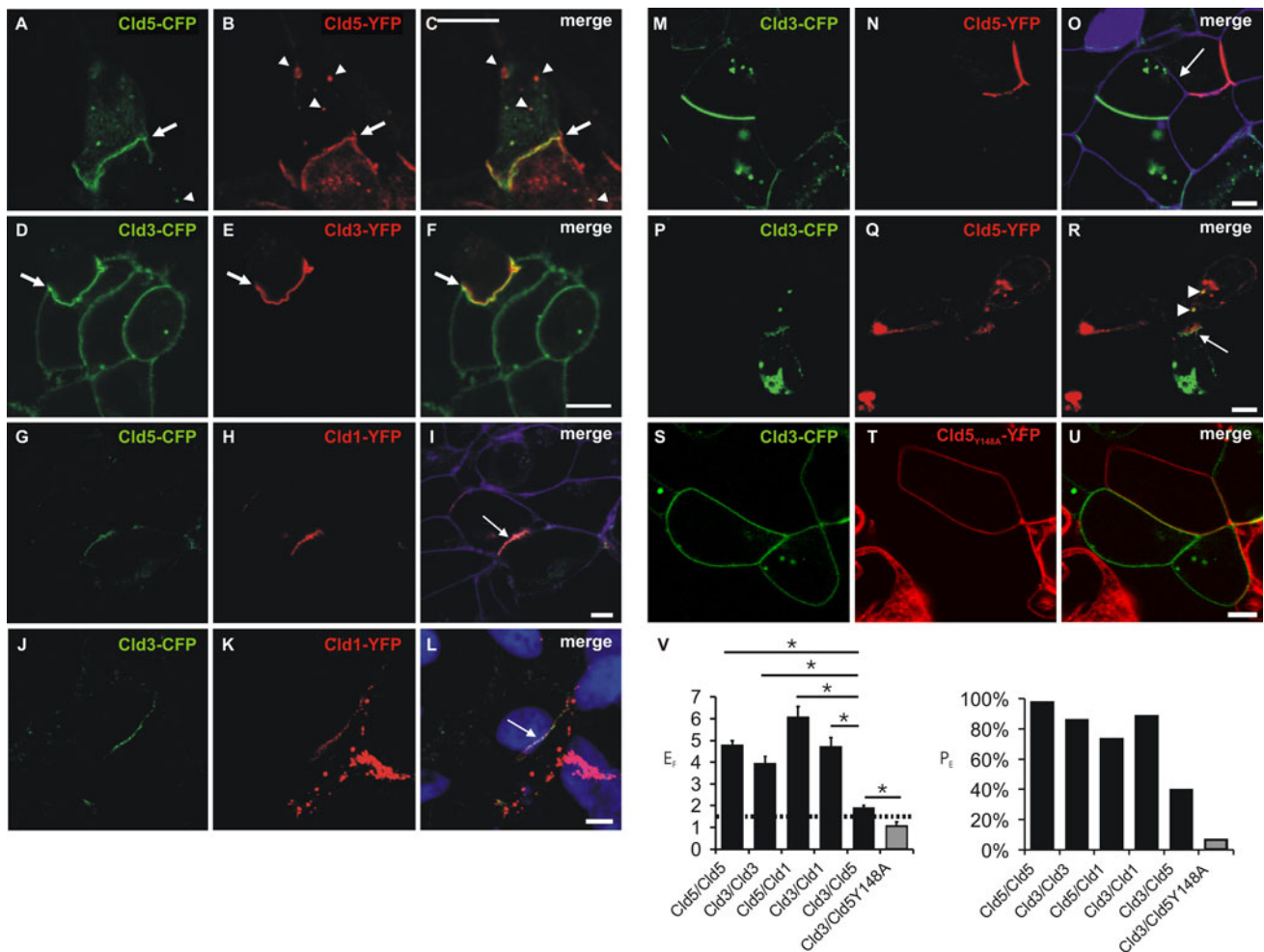


Fig. 3 Heterophilic *trans*-interaction between claudins. Confocal microscopy of cocultures of cells monotransfected with Cld5-CFP/Cld5-YFP (a–c), Cld3-CFP/Cld3-YFP (d–f), Cld5-CFP/Cld1-YFP (g–i), Cld3-CFP/Cld1-YFP (j–l), Cld3-CFP/Cld5-YFP (m–r), or Cld3-CFP/Cld5^{Y148A}-YFP (s–u). CFP- (green) and YFP- fluorescence (red) was imaged (a–u) and, partly, the plasma membrane visualized with trypan blue (i, o; violet) or nuclei stained with DAPI (l, blue). Strong colocalization and coenrichment of claudins at cell contacts (arrows) was detected at homologous (Cld5/Cld5, a–c, Cld3/Cld3, d–f) and heterologous cell contacts for Cld1/Cld5 (g–i) and Cld1/Cld3 (j–l). At contacts between Cld3- and Cld5-expressing cells, coenrichment was found to be weaker and less frequent (example without (m–o, arrow) and with (p–r, arrow) coenrichment). Cld3-CFP

containing vesicles (r, arrow heads) were detected in Cld5-YFP-expressing cells similar as Cld5-YFP containing vesicles (a–c, arrow heads) in Cld5-CFP-expressing cells and vice versa. At contacts between Cld3- and Cld5-Y148-expressing cells, no coenrichment was found (s–u). v Quantification of contact coenrichment. For Cld5/Cld5, Cld3/Cld3, Cld1/Cld3 and Cld1/Cld5 the factor of contact enrichment (E_F) was significantly higher than for Cld3/Cld5 and for Cld3/Cld5 than for Cld3/Cld5^{Y148A} that showed E_F similar to the negative control (Fig. 1). Similar differences were obtained for percentage of contacts with enrichment (P_E). Bar, 5 μ m. * $p < 0.01$; $n \geq 35$; mean + SEM; dotted line, threshold above *trans*-interaction is considered

Freeze-fracture electron microscopy revealed claudin subtype-specific characteristics of formation of tight junction strands

Cld5 strands are known to appear as discontinuous chains of intramembranous particles that are associated with the exoplasmic face (E-face) of the plasma membrane [29]. We reproduced this finding (Fig. 7a) and verified that non-tagged and YFP-tagged Cld5 form strands of similar morphology [3]. Also, we reproduced earlier reports [13] that Cld3, in contrast to Cld5, forms continuous strands

with intramembranous particles associated with the protoplasmic face (P-face) of the plasma membrane. In contrast, grooves with very few particles are found on the E-face (Fig. 7b). Coexpression of Cld3 and Cld5 resulted in strands with a mixed phenotype: discontinuous chains of intramembranous particles on the P-face as well as on the E-face (Fig. 7c). In addition, the substitution Y147A in Cld3, that strongly inhibits *trans*-interaction, abolished the formation of strands. Similarly for Cld12, which showed no strong *trans*-interactions (Fig. 1), no strands were detected after transfection of HEK cells (Fig 7d).

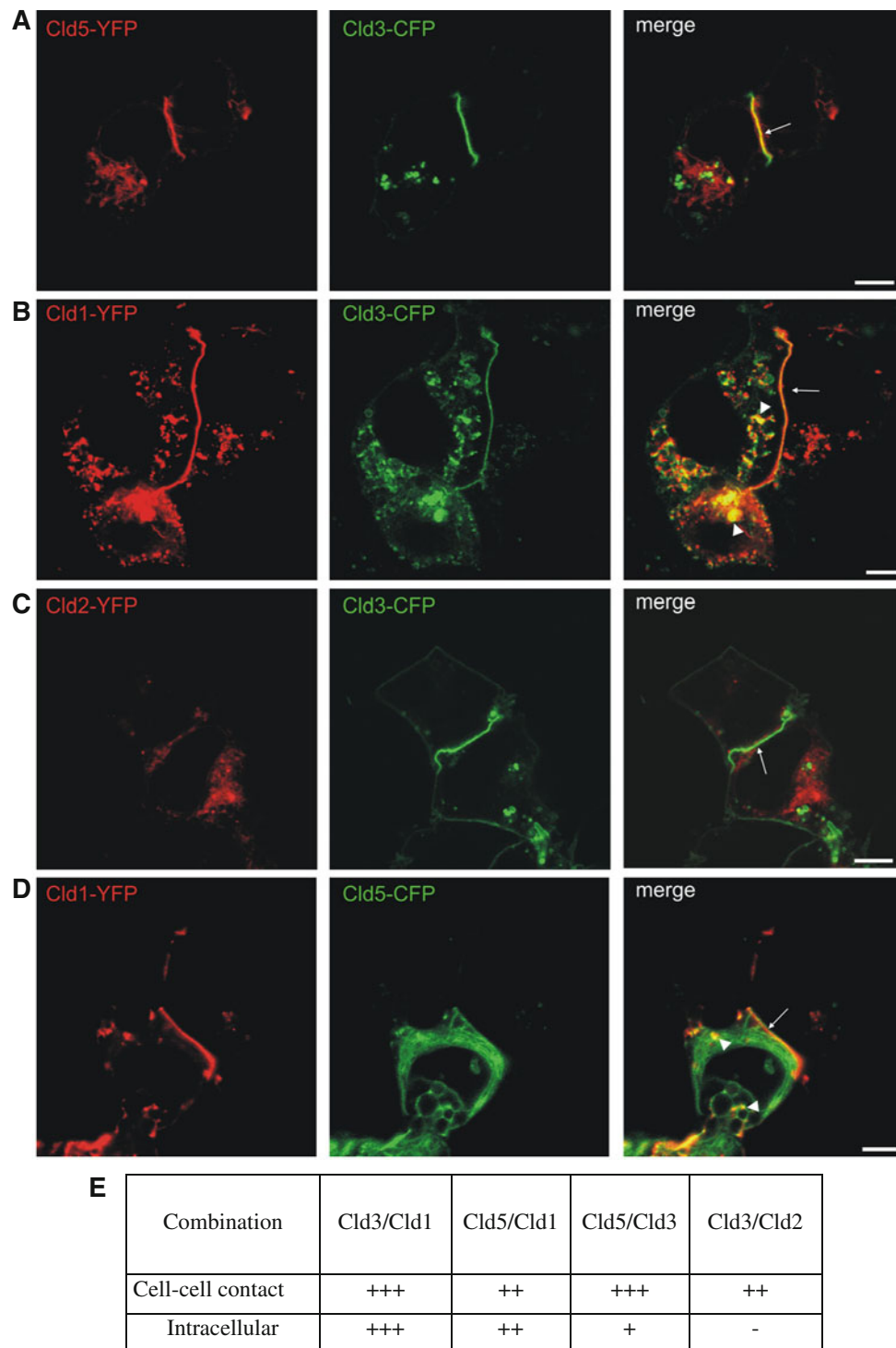


Fig. 4 Differential colocalization of coexpressed claudin subtypes at cell–cell contacts and intracellular compartments. Pairs of Cld1, -2, -3, and -5 were coexpressed in HEK cells and the subcellular distribution analyzed by confocal microscopy. At contacts between two Cld-expressing cells (*arrows*) colocalization of Cld3/Cld5 (**a**), Cld3/Cld1 (**b**), Cld5/Cld1 (**d**), and partly Cld3/Cld2 (**c**) was observed.

Strong colocalization in intracellular compartments (*arrow heads*) was found for Cld3/Cld1 (**b**), partially for Cld5/Cld1 (**d**) but not for Cld3/Cld5 (**a**) and Cld3/Cld2 (**c**). *Bar*, 5 μm (**e**) Summary of the colocalization analysis. –, no; (+)/+, weak; ++/+++, strong colocalization

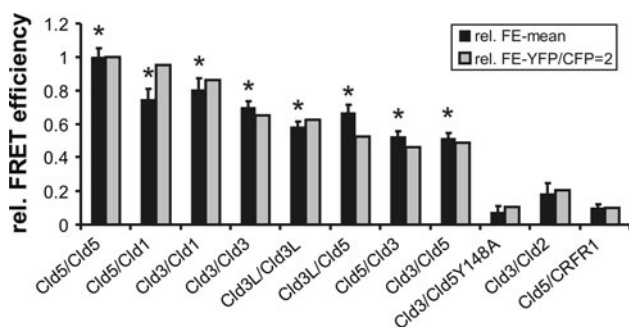


Fig. 5 Claudin subtype-specific differences in homo- and heterophilic *cis*-interactions of claudins at cell–cell contacts. HEK cells were cotransfected with YFP- and CFP-fusion proteins (given as CFP/YFP pairs). Fluorescence resonance energy transfer (FRET) at cell–cell contacts was analyzed in living cells by acceptor photobleaching. Relative FRET-efficiency (rFE, $F_{E\text{sample}}/F_{E\text{Cld5/Cld5}}$, black columns) and rFE normalized to YFP/CFP fluorescence intensity ratio = 2 (gray columns) using logarithmic regression (see “Methods”). Mean + SEM; $n = 20\text{--}50$; * $p < 0.01$ compared to Cld5/CRFR1; Cld3L, Cld3 with linker

These results demonstrate that *trans*-interaction is a prerequisite for strand formation. All together, the data demonstrate claudin subtype-specific characteristics of strand formation.

The mobility of claudins is subtype-specific and affected by *trans*-interaction

The mobility of claudins was analyzed by fluorescence recovery after photobleaching, FRAP [21]. At cell–cell contacts of HEK cells stably transfected with claudin-YFP constructs, Cld5 showed a mobile fraction of $32 \pm 2\%$, only, whereas Cld3 exhibited a mobile fraction of $73 \pm 7\%$ ($p < 0.01$; Fig. 8a–c). In addition, the $t_{1/2}$ of recovery for Cld5 (33 ± 4 s) was nearly twice as long as that of Cld3 (19 ± 2 s; $p < 0.01$; Fig. 8d). The substitution Y148A in Cld5 resulted in a much higher mobile fraction $57 \pm 10\%$ ($p < 0.05$), and shorter $t_{1/2}$ (17 ± 4 s; $p < 0.05$; Fig. 8c, d) that were not significantly different from mobile fraction and $t_{1/2}$ of Cld3. Cld5 was far more mobile within plasma membrane areas away from cell–cell contacts (mobile fraction $61\% \pm 3\%$; $t_{1/2}$ 16 ± 3 s) than at cell–cell contacts ($p < 0.02$ for each vs. Cld5 at cell contacts). This was similar to FRAP behavior of intracellular Cld5 (mobile fraction $58 \pm 3\%$; $t_{1/2}$ 18 ± 5 s) as well as Cld5_{Y148A} at cell–cell contacts. In contrast to Cld5, exchange behavior of Cld3 within plasma membrane areas away from cell–cell contacts (mobile fraction $72 \pm 4\%$; $t_{1/2}$ 18 ± 2 s) was similar to that at cell–cell contacts. These data indicate that *trans*-interactions of Cld5 at cell–cell contacts and presumably incorporation of Cld5 in strands limits its mobility. The

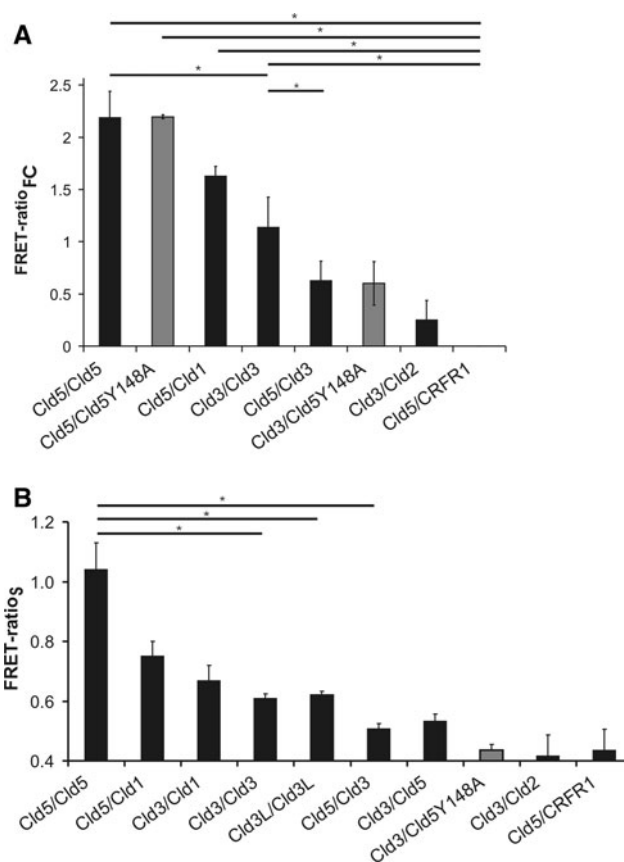


Fig. 6 Claudin subtype-specific differences in homo- and heterophilic *cis*-interactions in cell suspension. HEK cells were cotransfected with CFP- and YFP-fusion proteins (e.g., Cld5CFP/Cld5YFP), detached from the culture plate and single cell suspension prepared by pipetting. **a** FRET-analysis by flow cytometry. As a measure for the FRET-efficiency, the FRET-ratio_{FC} was calculated. * $p < 0.02$, $n = 3\text{--}5$, for each sample $>2,500$ coexpressing cells were analyzed. **b** FRET-analysis by spectrofluorometry. As a measure for the FRET-efficiency, the FRET-ratio_S was calculated. In addition to indicated pairs, the FRET-ratio_S was for all pairs but not Cld3/Cld2 and Cld3/Cld5_{Y148A} significantly higher than for the negative control (Cld5/CRFR1). * $p < 0.01$, $n = 4\text{--}16$

mobility in the plasma membrane is higher for Cld3 than for Cld5. This could be due to a higher amount of non-polymerized Cld3 in the plasma membrane or due to higher disassembly/assembly rate of the strands for Cld3 relative to Cld5.

Claudins form diffusion barriers at cell–cell contacts

To analyze the barrier function of reconstituted TJ-strands, claudin-expressing HEK cells were incubated with the plasma membrane stain CellMask™ and analyzed by life cell imaging. Incubation with $5 \mu\text{g/ml}$ for 15 min or with $0.25 \mu\text{g/ml}$ for 20 min labeled the plasma membrane everywhere. In contrast, incubation with $0.25 \mu\text{g/ml}$ CellMask for 5 min resulted in a strong labeling of

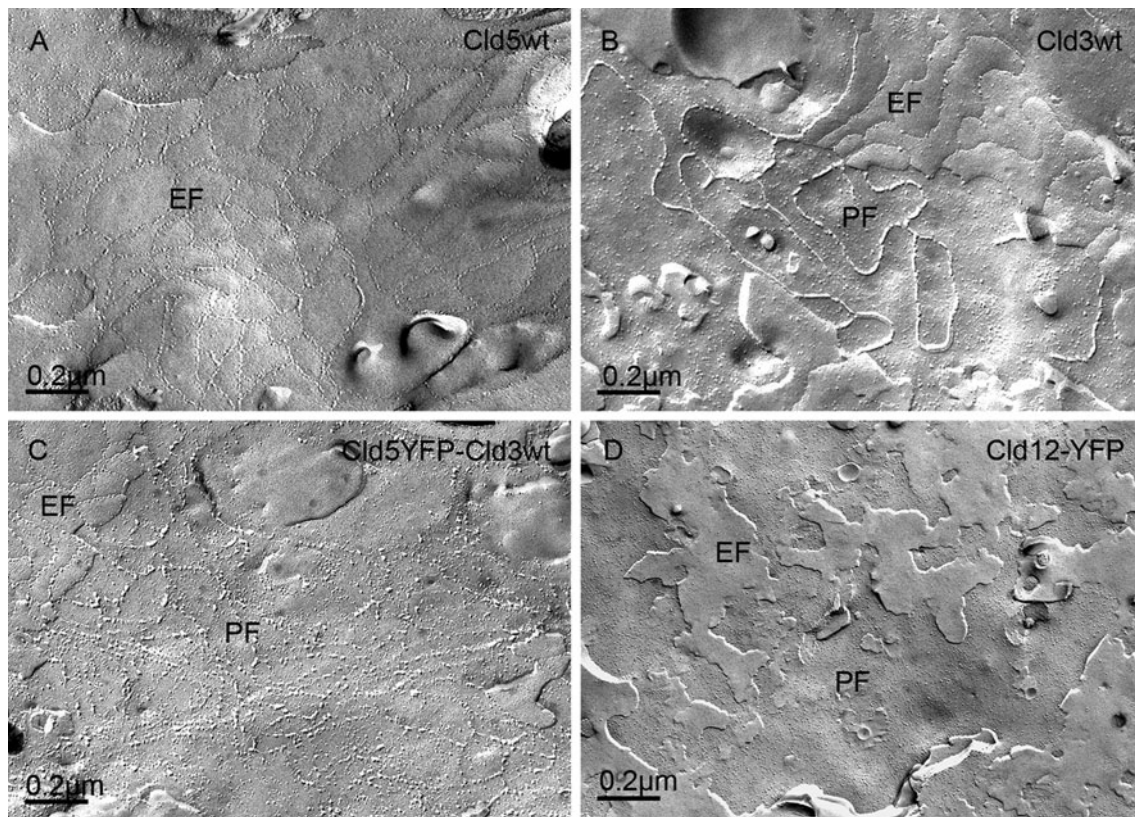


Fig. 7 Claudin subtype-specific characteristics of formation of tight junction strands. Claudin-transfected HEK cells were analyzed by freeze-fracture electron microscopy. For Cld5_{wt}-expressing cells, discontinuous strands with intramembranous particles associated with the exoplasmic face (E-face) of the plasma membrane were detected (a). For Cld3_{wt}-expressing cells, continuous strands associated with

the protoplasmic face (P-face) of the plasma membrane were detected (b). For cells that coexpress Cld5_{wt}-YFP and Cld3_{wt}, intramembranous particles were found on the E- as well as on the P-face (c). For cells transfected with Cld12 (d), Cld3_{Y147A} or non-transfected cells (latter not shown), and for non-transfected cells, no tight junction strands were observed

contacts without claudin enrichment but not of contacts with claudin enrichment (Fig. 9, Fig. S5). This was found for contacts between two Cld3-expressing or two Cld5-expressing but not for CRFR1-expressing cells (Fig. 9a–c). In addition, no clear CellMask™-labeling was found for contacts between two Cld3/Cld5-coexpressing cells (Fig. 9d). This demonstrates that the TJ-strands that are reconstituted by expression of Cld3 and/or Cld5 form a diffusion barrier which CO which inhibits membrane incorporation of an extracellularly administered marker.

Discussion

The molecular mechanisms that result in the formation of membranous TJ-strands are not understood. Here, we show claudin subtype-specific characteristics with respect to *cis*- and *trans*-interaction as well as formation of TJ-strands. Furthermore, we provide a model for the formation of heteropolymeric strands (Fig. 10).

Homophilic claudin interactions

Previously, we adapted a cellular reconstitution assay [30] to analyze the formation of TJ-strands on the molecular level. Instead of polarized epithelial or endothelial cells, HEK cells that do not form endogenous TJ were transfected with Cld5-CFP/YFP or mutants thereof to reconstitute defined claudin polymers [3]. Homophilic *trans*-interaction was detected by enrichment of Cld5 at contacts between two Cld5-expressing cells. Using this assay, we here describe that Cld1, -3, and -5, which belong to the group of classic claudins [5] show a similar capability for homophilic *trans*-interaction. This is consistent with earlier studies [10, 13].

In contrast, the non-classic Cld12 did not show considerable homophilic *trans*-interaction. Consistently, Cld12 did not form homopolymeric strands as do the classic claudins. However, it can not be excluded that the C-terminal YFP-tag prevents strand formation for Cld12 but not for classic claudins. The non-classic claudins show strong sequence differences compared to the classic claudins (e.g.,

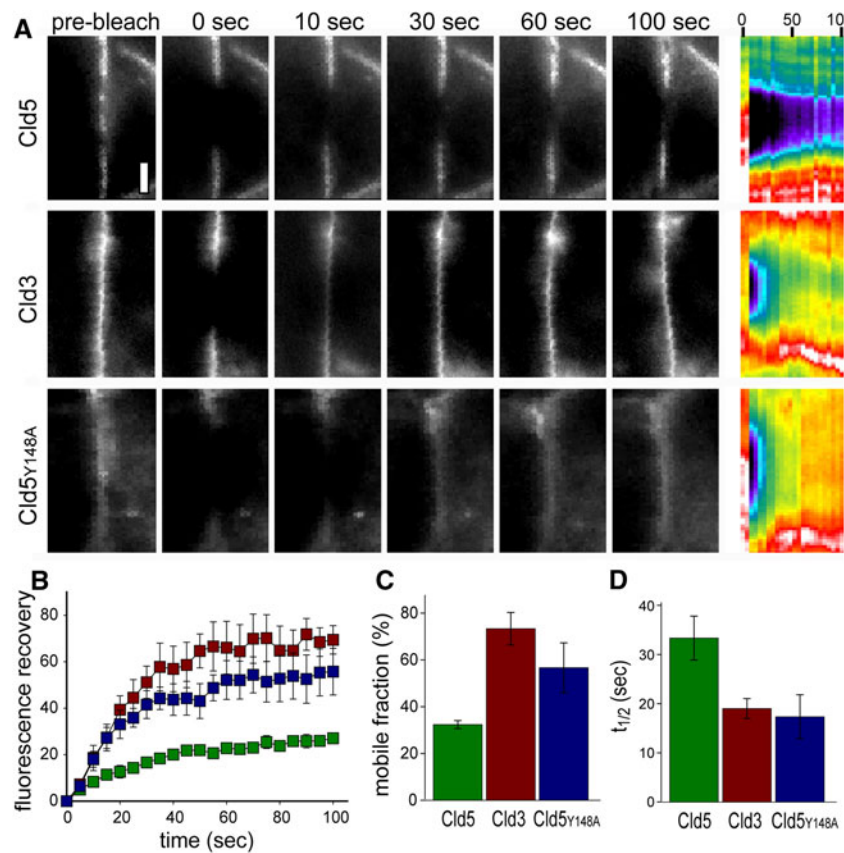


Fig. 8 Mobility of claudins is subtype-specific and affected by *trans*-interaction. **a** FRAP behavior of Cld5, Cld3, and Cld5_{Y148A} at areas of cell–cell contact between HEK cells stably transfected with the respective YFP fusion constructs. Individual images are shown as indicated, with the corresponding kymograph at the right. Bar = 2 μ m. **b** Recovery curves for Cld5, Cld3 and Cld5_{Y148A} at

areas of cell–cell contact ($n = 3$ per condition). **c** Mobile fractions of Cld5, Cld3 and Cld5_{Y148A} at areas of cell–cell contact calculated from recovery data in **b** ($n = 3$ per condition). **d** $t_{1/2}$ of Cld5, Cld3, Cld5_{Y148A} recovery at areas of cell–cell contact calculated from data in **b** ($n = 3$ per condition)

Cld12 contains no aromatic residue corresponding to Y148 in Cld5 and Y147 in Cld3 [5]). Similar to Cld12, the non-classic Cld16 does not form homopolymeric strands [7]. However, the non-classic Cld11 is able to form homopolymeric strands [31]. We show that inhibition of *trans*-interactions, by removing a conserved aromatic side chain in the ECL2 of classic claudins, diminished strand formation as shown for Cld5 [3] and Cld3 (Figs. 2, 7). In addition, *trans*-interactions reduce the mobility of Cld5 (Fig 8). Therefore, we conclude that *trans*-interactions are necessary for strand formation, as discussed earlier [3] and propose that Cld12 and possibly other non-classic claudins lack the ability to form homopolymeric strands due to the lack of ability for homophilic *trans*-interaction.

Comparison of homo- and heterophilic *trans*-interactions

To understand the barrier properties of TJ on the molecular level, it is necessary to analyze the heterophilic compatibility

of claudins. Heterophilic *trans*-interactions (heterotypic interactions) have been reported for Cld1/-3, -2/-3, -3/-5 but not for Cld1/-2, -3/-4, -4/-5, -1/-4, -16/-19, -1/-10b and -1/-15 [7, 10, 13, 32]. Heterophilic *cis*-interactions (heteromeric interactions) have been reported for Cld3 and Cld4 pairs [10] and Cld16 and Cld19 pairs [7]. Heterophilic interactions that could not be clearly distinguished as *cis*- or *trans*- were noted for Cld1/2, Cld1/Cld3 and Cld2/Cld3 [13, 33], but the only determinants of *cis*-interactions identified thus far were G20, Q57, and G123 in human Cld19, which mediate *cis*-interactions with Cld16 [7].

For the blood–brain barrier Cld1, -3 and -5 are relevant [6, 14]. We found the capability for heterophilic *trans*-interactions of Cld5/Cld1 and Cld3/Cld1 to be as pronounced as that for homophilic Cld5/Cld5 and Cld3/Cld3 interactions. In contrast, Cld3/Cld5 *trans*-interactions were much less pronounced, although still significantly stronger than the negative control. The Cld3/Cld1 interaction is consistent with earlier studies [10, 13, 33]. Also similar to our data, the Cld5/Cld5 interaction has been reported to be stronger than Cld3/

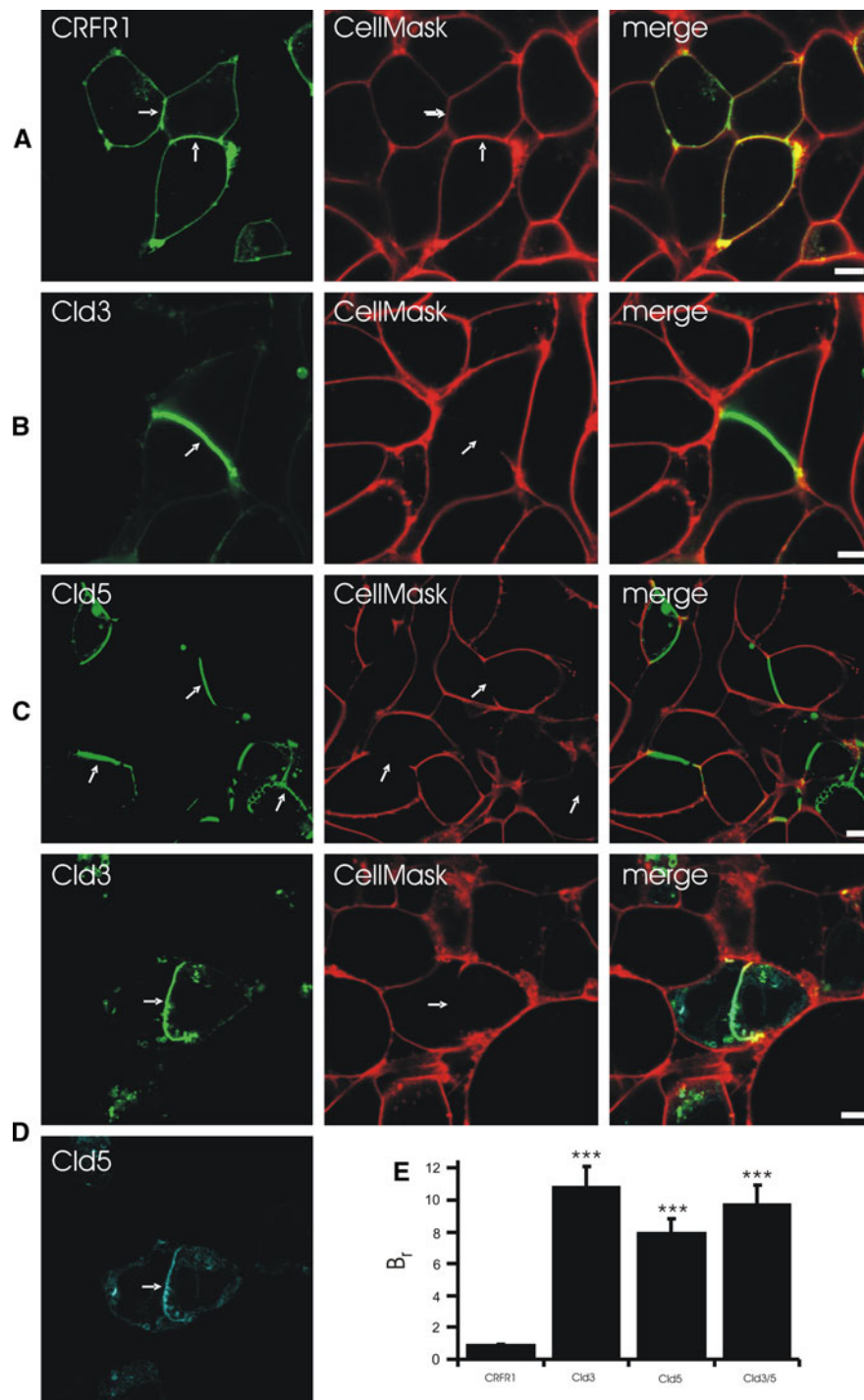
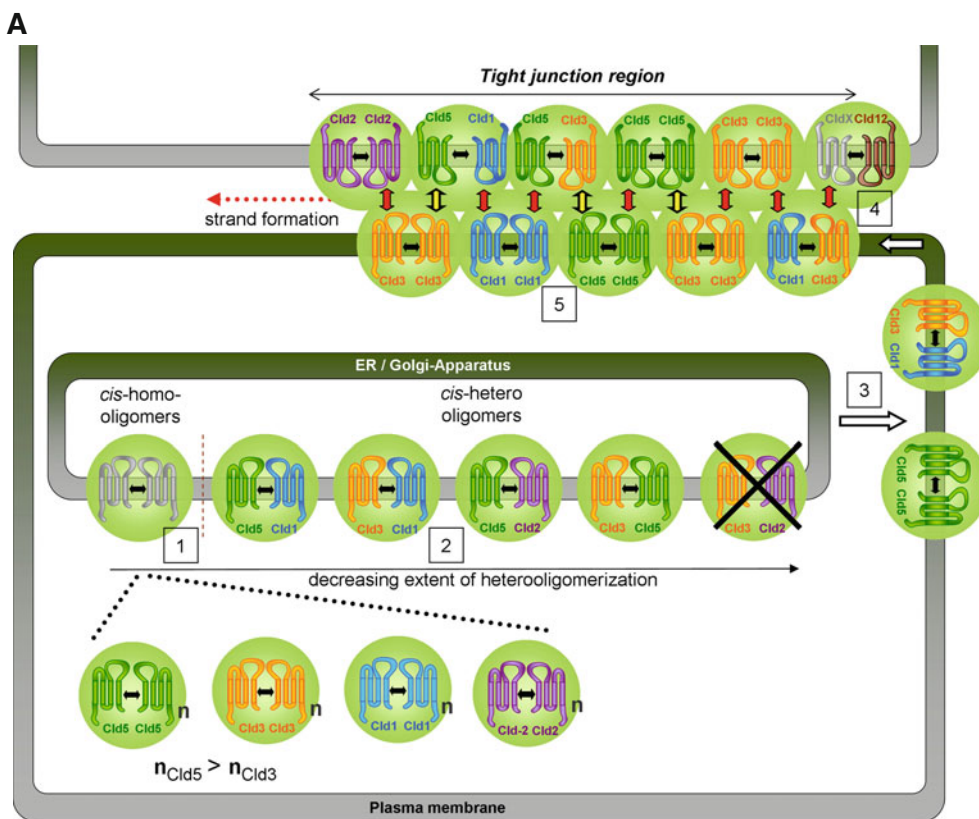


Fig. 9 Claudins form diffusion barrier at contacts between claudin-expressing HEK cells. Cells were incubated with CellMask for 5 min and the labeling of the cell membrane was analyzed by confocal microscopy. **a** CellMask labeled contacts between CRFR1-CFP(control)-expressing and non-expressing cells as well as contacts between two CRFR1-CFP-expressing cells. At contacts between Cld3-YFP-

(**b**), Cld5-YFP (**c**) or Cld3-YFP/Cld5-CFP- (**d**) expressing cells, CellMask labeling was much weaker or absent. **e** The barrier ratio (B_t), as a measure for paracellular barrier preventing CellMask labeling, was determined using confocal intensity profiles. *Bar*, 5 μm ; $***p < 0.001$ versus CRFR1; *arrows*, contacts between cells expressing fusion proteins

Cld5 interaction [10]. However, in contrast to our results, the latter authors did not detect *trans*-interactions between Cld5 and Cld1. This difference could be due to the use of human

Cld1 and human Cld5, while we used human Cld1 and mouse Cld5. We also obtained similar results for mouse Cld1 and mouse Cld5 (data not shown). Therefore, although species



B Compatibility of classic claudin subtypes relevant for cerebral barriers

	Cld1	Cld2	Cld3	Cld5
Cld1	c+ / t+	nd / t-	c+ / t+	c+ / t+
Cld2	nd / t-	c+ / t+	c- / t+	(c+)/ nd
Cld3	c+ / t+	c- / t+	c+ / t+	c+ / t+
Cld5	c+ / t+	(c+)/ nd	c+ / t+	c+ / t+

Fig. 10 a Model of formation and molecular organization of heteropolymeric claudin strands. Cld1, -2, -3, -5, and -12, assumed to be expressed at cerebral barriers, are shown. *Black double arrows*, *cis*-interaction; *green spheres*, *cis*-oligomers; *n*, number of molecules; *red arrows*, homo- and heterophilic *trans*-interactions; *black/yellow arrows*, Cld3/Cld5 *trans*-interactions; CldX, claudin that incorporates

Cld12 by heterophilic *trans*- or *cis*-interaction. **b** Compatibility of classic claudin subtypes relevant for cerebral barriers. *c*, *cis*-interaction; *t*, *trans*-interaction; *+*, compatible; *-*, incompatible. *Bracket*, detected intracellularly, only; *nd*, not determined; *blue*, according to [13, 36, 37], 1–5, see text

variation cannot be excluded, the data and fact that sequence similarity between mouse and human is >94% suggest that species effects are unlikely to explain differences of the data. However, the discrepancy could be due to other methodological issues. For example, Daugherty et al. [10] used, in contrast to us, claudin constructs that could bind to proteins containing PDZ-domains, e.g., ZO-1. This could change the subcellular distribution of claudins. Moreover, the use of chemically fixed cells could disturb some interactions. Finally, although the coimmunoprecipitation approach used by Daugherty et al. is a powerful technique, it cannot exclude a loss of interactions between transmembrane proteins after detergent solubilization. In contrast, we analyzed claudins in living cells allowing investigation of interactions under

physiological conditions. However, it must also be recognized that our assays do not detect physical association but trace interactions by indirect parameters such as contact-enrichment, TJ-strand formation and FRET.

Claudin subtype-specific *cis*-interactions

At contacts between claudin-coexpressing cells, colocalization was found for Cld3/Cld5, Cld5/Cld1, Cld3/Cld1 and partly for Cld3/Cld2. However, the different claudin pairs showed striking differences in their intracellular codistribution. Intracellular colocalization was commonly found for Cld1/Cld3, partially for Cld1/Cld5, infrequently for Cld3/Cld5, and very infrequently for Cld2/Cld3. The subtype-

specific differences in colocalization suggest that the subcellular distribution is caused by subtype-specific interactions rather than by undirected aggregation. The claudin-containing intracellular compartments did not considerably colocalize with markers for endosomes or lysosomes but partly with those for the endoplasmic reticulum (Fig. S4).

Because of the different extent of colocalization at cell–cell contacts and at intracellular compartments, we performed FRET-analysis independently at and away from cell–cell contacts. At cell–cell contacts and therefore presumably in TJ-strands, *cis*- and *trans*-interactions are likely formed. There, FRET-efficiencies decreased in the order Cld5/Cld5, Cld5/Cld1, Cld3/Cld1 > Cld3/Cld3 ≥ Cld3/Cld5 and no FRET for Cld3/Cld2. In single cell suspensions, cell–cell contacts and in turn *trans*-interactions are assumed to be absent. Those FRET-efficiencies decreased in the order Cld5/Cld5 > Cld5/Cld1 > Cld3/Cld3 > Cld3/Cld5, with no FRET found for Cld3/Cld2. This indicates that *cis*-interactions between claudin pairs are similar outside and inside TJ-strands.

However, especially for Cld3/Cld5, important differences have been found: First, Cld3 and Cld5 demonstrated marked colocalization at cell–cell contacts, but not outside of contacts. Second, the FRET-efficiency of Cld3/Cld5 at cell contacts is closer to that of Cld3/Cld3 than is the FRET efficiency of Cld3/Cld5 outside of contacts. Finally, Cld3/Cld5-, but not Cld5/Cld5- [3], FRET is abolished by Y148A substitution in Cld5 (inhibition of *trans*-interactions) at cell contacts, but this substitution has no effect on *cis*-interactions measured in suspension.

These results indicate that *trans*-interactions are necessary for the FRET between Cld3 and Cld5. However, this FRET is unlikely to be due to direct energy transfer between *trans*-interacting Cld3 and Cld5 on opposing plasma membranes because the distance between the respective intracellular CFP- and YFP-tags is too big (>8 nm) for efficient FRET [34]. It is also unlikely that Y148A inhibits Cld3/Cld5 but not Cld5/Cld5 *cis*-interactions. Hence, the data suggest that the FRET-signal and, in turn, the spatial proximity between Cld3 and Cld5 in one membrane at cell–cell contacts is promoted by homo- and/or heterophilic *trans*-interactions rather than by direct *cis*-interactions.

Previously, some heterophilic *cis*-interactions between claudin subtypes have been analyzed by coimmunoprecipitation after cell lysis [10, 33]. Although this approach has provided important data, potential artifacts might occur due to detergent solubilization. In addition, immunofreeze-fracture microscopy of strands with two different labels was applied [13]. Although this technique is very powerful, the spatial resolution is still limited due to the size of antibodies and gold particles and a potential contribution of *trans*-interactions to colocalization of claudins in strands has to be considered. An effective split ubiquitin assay in

yeast was used to analyze *cis*-interactions independent of *trans*-interactions [7]. However, yeast lack mammalian characteristics including contacts between plasma membranes. Hence, *cis*- and *trans*-interactions cannot be effectively compared in this system.

We complemented the above-mentioned assays by FRET-experiments with HEK cells within and outside of reconstituted TJ-strands. For an efficient FRET-analysis outside of strands, we here developed a new method based on flow cytometry. Similar FRET techniques have been used before [25, 26]. We improved and optimized the method, especially, with consideration of the strong dependence of the FRET-efficiency on the acceptor/donor ratio and the characteristics of junctional proteins.

Reconstituted TJ-strands form a functional diffusion barrier

Claudins are able to reconstitute TJ-strands in non-polar cells [3, 30]. Nevertheless, these strands do not form a continuous sealing belt around the cells as in epi-/endothelial cells. This is probably due to the lack of cytoplasmic TJ-proteins. Hence, standard Transwell assays to analyze paracellular permeability are hindered in such reconstitution systems. To overcome this limitation we developed a novel, imaging-based assay to demonstrate and quantify barrier functions of reconstituted and molecular defined TJ-strands. We showed that a single claudin (e.g., Cld3 or Cld5) is sufficient to form a diffusion barrier. Whether the diffusion is inhibited in the paracellular space and/or within the membrane might be analyzed by continuative experiments including the novel assay.

Model of formation and molecular organization of heteropolymeric claudin strands

The results obtained and data from the literature [10, 13, 33, 35–37] were combined to propose a model of heteropolymeric strands for Cld1, -2, -3, -5, and -12 that are expressed at cerebral barriers (Fig. 10):

- (1) Two to six [33, 35] claudin molecules might form oligomers mediated by *cis*-interactions in intracellular compartments. This is demonstrated by FRET in cell suspensions of Cld-CFP/Cld-YFP-coexpressing cells in which most of the claudins are present in intracellular compartments. This conclusion is supported by FRET analysis of intracellular compartments using confocal microscopy (Fig. S3).
- (2) Differences in the FRET-efficiency suggest that *cis*-interactions in intracellular compartments are differentially pronounced in the order: Cld5/Cld5 > Cld5/Cld1 > Cld3/Cld1 > Cld3/Cld3 > Cld3/Cld5, and

that *cis*-interactions do not occur between Cld3/Cld2. The higher FRET-efficiency for Cld5- compared to Cld3-homooligomers supports the conclusion that Cld5-*cis*-homooligomers are sterically different from Cld3-*cis*-homooligomers, e.g., higher number of molecules ($n_{\text{Cld5}} > n_{\text{Cld3}}$). This is consistent with differences in oligomer size detected by PFO-PAGE [33]. Evidence for homophilic *cis*-interaction of Cld1 was recently provided by FRET-assays [37]. Due to strong sequence homology among classic claudins [5], Cld2 is also assumed to form *cis*-oligomers.

- (3) The *cis*-oligomers are transported to the plasma membrane and diffuse to cell–cell contacts.
- (4) At cell–cell contacts, *trans*-interactions trigger formation of polymeric strands, as proposed earlier [3]. Homophilic *trans*-interactions are possible for Cld1, -3, -5, and -2 [13], but not for Cld12. Heterophilic Cld3/Cld5 *trans*-interactions are less pronounced than heterophilic Cld3/Cld1 and Cld5/Cld1 and all homophilic *trans*-interactions investigated. Nevertheless, heterophilic Cld3/Cld5 *trans*-interactions (Fig. 10, black/yellow arrows) may be essential to form functional heteropolymers, since these are necessary for Cld3/Cld5 colocalization and FRET. Heterophilic Cld3/Cld2, but not Cld1/Cld2, *trans*-interactions were described [13].

Aromatic residues in the ECL2 that are conserved between classic claudins (e.g., Y148 in mCld5, Y147 in mCld3) are essential for homo- as well as heterophilic *trans*-interactions but not for the assembly of *cis*-oligomers.

- (5) In TJ-strands, spatial proximity of claudins in one membrane due to *cis*-interactions and/or *trans*-interactions occurs in the order of preference: Cld5/Cld5 > Cld5/Cld1, Cld3/Cld1, Cld3/Cld3 > Cld3/Cld5 > Cld3/Cld2.

In contrast to the classic claudins, the non-classic Cld12 is not able to form homophilic *trans*-interactions or homopolymeric strands. Probably, heterophilic *cis*- and/or *trans*-interactions with another TJ-protein are necessary for the incorporation of Cld12 in strands. The interactions depicted in the model (Fig. 10) are consistent with the data.

Freeze-fracture electron microscopy demonstrated claudin subtype-specific characteristics of TJ-strands. Coexpression of Cld3 and Cld5 resulted in strands with a phenotype that represent a mixture of that of Cld3- (P-face) and Cld5-homopolymers (E-face): discontinuous chains of intramembranous particles on the P-face as well as on the E-face. This resembles TJ in endothelia of the blood–brain barrier in vivo. There, the expression of Cld3 together with Cld5 was reported to correlate with mixed P-/E-face

association and high tightness of brain endothelial cell junctions [14, 15, 38]. Here, we demonstrate that this functionally important ultrastructural characteristic is indeed due to the formation of Cld3/Cld5 heteropolymeric strands and does not require other blood–brain barrier-specific factors since we observed it in HEK-cells that do not possess blood–brain barrier properties.

In summary, we provide novel mechanistic insights into the principles that define molecular organization of TJ-strands. This improves the understanding of paracellular barriers and might be used to develop new strategies to improve drug delivery across cerebral barriers, e.g., by modulation of the Cld3/Cld5 interaction.

Acknowledgments We gratefully acknowledge the help of Ria Knittel in freeze-fracturing. This work was funded by DFG BL308/7-3, 7-4 and PI 837/2-1 and NIH DK61931.

References

1. Angelow S, Ahlstrom R, Yu AS (2008) Biology of claudins. *Am J Physiol Renal Physiol* 295:F867–F876
2. Staehelin LA (1974) Structure and function of intercellular junctions. *Int Rev Cytol* 39:191–283
3. Piontek J, Winkler L, Wolburg H, Muller SL, Zuleger N, Piehl C, Wiesner B, Krause G, Blasig IE (2008) Formation of tight junction: determinants of homophilic interaction between classic claudins. *FASEB J* 22:146–158
4. Morita K, Furuse M, Fujimoto K, Tsukita S (1999) Claudin multigene family encoding four-transmembrane domain protein components of tight junction strands. *Proc Natl Acad Sci USA* 96:511–516
5. Krause G, Winkler L, Mueller SL, Haseloff RF, Piontek J, Blasig IE (2008) Structure and function of claudins. *Biochim Biophys Acta* 1778:631–645
6. Nitta T, Hata M, Gotoh S, Seo Y, Sasaki H, Hashimoto N, Furuse M, Tsukita S (2003) Size-selective loosening of the blood–brain barrier in claudin-5-deficient mice. *J Cell Biol* 161:653–660
7. Hou J, Renigunta A, Konrad M, Gomes AS, Schneeberger EE, Paul DL, Waldegger S, Goodenough DA (2008) Claudin-16 and claudin-19 interact and form a cation-selective tight junction complex. *J Clin Invest* 118:619–628
8. Hou J, Renigunta A, Gomes AS, Hou M, Paul DL, Waldegger S, Goodenough DA (2009) Claudin-16 and claudin-19 interaction is required for their assembly into tight junctions and for renal reabsorption of magnesium. *Proc Natl Acad Sci USA* 106:15350–15355
9. Yu AS, Cheng MH, Angelow S, Gunzel D, Kanzawa SA, Schneeberger EE, Fromm M, Coalson RD (2009) Molecular basis for cation selectivity in claudin-2-based paracellular pores: identification of an electrostatic interaction site. *J Gen Physiol* 133:111–127
10. Daugherty BL, Ward C, Smith T, Ritzenthaler JD, Koval M (2007) Regulation of heterotypic claudin compatibility. *J Biol Chem* 282:30005–30013
11. Piehl C, Piontek J, Cording J, Wolburg H, Blasig IE (2010) Participation of the second extracellular loop of claudin-5 in paracellular tightening against ions, small and large molecules. *Cell Mol Life Sci* 67:2131–2140

12. Zhang J, Piontek J, Wolburg H, Piehl C, Liss M, Otten C, Christ A, Willnow TE, Blasig IE, Abdelilah-Seyfried S (2010) Establishment of a neuroepithelial barrier by Claudin5a is essential for zebrafish brain ventricular lumen expansion. *Proc Natl Acad Sci USA* 107:1425–1430
13. Furuse M, Sasaki H, Tsukita S (1999) Manner of interaction of heterogeneous claudin species within and between tight junction strands. *J Cell Biol* 147:891–903
14. Wolburg H, Lippoldt A (2002) Tight junctions of the blood–brain barrier: development, composition and regulation. *Vascul Pharmacol* 38:323–337
15. Kniesel U, Risau W, Wolburg H (1996) Development of blood–brain barrier tight junctions in the rat cortex. *Dev Brain Res* 96:229–240
16. Liebner S, Fischmann A, Rascher G, Duffner F, Grote EH, Kalbacher H, Wolburg H (2000) Claudin-1 and claudin-5 expression and tight junction morphology are altered in blood vessels of human glioblastoma multiforme. *Acta Neuropathol* 100:323–331
17. Wolburg H, Wolburg-Buchholz K, Kraus J, Rascher-Eggstein G, Liebner S, Hamm S, Duffner F, Grote EH, Risau W, Engelhardt B (2003) Localization of claudin-3 in tight junctions of the blood–brain barrier is selectively lost during experimental autoimmune encephalomyelitis and human glioblastoma multiforme. *Acta Neuropathol* 105:586–592
18. Winkler L, Gehring C, Wenzel A, Muller SL, Piehl C, Krause G, Blasig IE, Piontek J (2009) Molecular determinants of the interaction between *Clostridium perfringens* enterotoxin fragments and claudin-3. *J Biol Chem* 284:18863–18872
19. Blasig IE, Winkler L, Lassowski B, Mueller SL, Zuleger N, Krause E, Krause G, Gast K, Kolbe M, Piontek J (2006) On the self-association potential of transmembrane tight junction proteins. *Cell Mol Life Sci* 63:505–514
20. Shen L, Weber CR, Turner JR (2008) The tight junction protein complex undergoes rapid and continuous molecular remodeling at steady state. *J Cell Biol* 181:683–695
21. Yu D, Marchiando AM, Weber CR, Raleigh DR, Wang YM, Shen L, Turner JR (2010) MLCK-dependent exchange and actin binding region-dependent anchoring of ZO-1 regulate tight junction barrier function. *Proc Natl Acad Sci USA* 107:8237–8241
22. Mack AF, Wolburg H (2006) Growing axons in fish optic nerve are accompanied by astrocytes interconnected by tight junctions. *Brain Res* 1103:25–31
23. Matsuda M, Kubo A, Furuse M, Tsukita S (2004) A peculiar internalization of claudins, tight junction-specific adhesion molecules, during the intercellular movement of epithelial cells. *J Cell Sci* 117:1247–1257
24. Wallrabe H, Elangovan M, Burchard A, Periasamy A, Barroso M (2003) Confocal FRET microscopy to measure clustering of ligand-receptor complexes in endocytic membranes. *Biophys J* 85:559–571
25. Banning C, Votteler J, Hoffmann D, Koppensteiner H, Warmer M, Reimer R, Kirchhoff F, Schubert U, Hauber J, Schindler M (2010) A flow cytometry-based FRET assay to identify and analyse protein–protein interactions in living cells. *Plos One* 5
26. van Wageningen S, Pennings AH, van der Reijden BA, Boezeman JB, de Lange F, Jansen JH (2006) Isolation of FRET-positive cells using single 408-nm laser flow cytometry. *Cytom Part A* 69A:291–298
27. Di WL, Gu Y, Common JEA, Aasen T, O’Toole EA, Kelsell DP, Zicha D (2005) Connexin interaction patterns in keratinocytes revealed morphologically and by FRET analysis. *J Cell Sci* 118:1505–1514
28. Amiri H, Schultz G, Schaefer M (2003) FRET-based analysis of TRPC subunit stoichiometry. *Cell Calcium* 33:463–470
29. Morita K, Sasaki H, Furuse M, Tsukita S (1999) Endothelial claudin: claudin-5/TMVCF constitutes tight junction strands in endothelial cells. *J Cell Biol* 147:185–194
30. Furuse M, Sasaki H, Fujimoto K, Tsukita S (1998) A single gene product, claudin-1 or -2, reconstitutes tight junction strands and recruits occludin in fibroblasts. *J Cell Biol* 143:391–401
31. Morita K, Sasaki H, Fujimoto K, Furuse M, Tsukita S (1999) Claudin-11/OSP-based tight junctions of myelin sheaths in brain and sertoli cells in testis. *J Cell Biol* 145:579–588
32. Inai T, Kamimura T, Hirose E, Iida H, Shibata Y (2010) The protoplasmic or exoplasmic face association of tight junction particles cannot predict paracellular permeability or heterotypic claudin compatibility. *Eur J Cell Biol* 89:547–556
33. Coyne CB, Gambling TM, Boucher RC, Carson JL, Johnson LG (2003) Role of claudin interactions in airway tight junctional permeability. *Am J Physiol Lung Cell Mol Physiol* 285:L1166–L1178
34. Sekar RB, Periasamy A (2003) Fluorescence resonance energy transfer (FRET) microscopy imaging of live cell protein localizations. *J Cell Biol* 160:629–633
35. Mitic LL, Unger VM, Anderson JM (2003) Expression, solubilization, and biochemical characterization of the tight junction transmembrane protein claudin-4. *Protein Sci* 12:218–227
36. Van Itallie CM, Mitic LL, Anderson JM (2010) Claudin-2 forms homodimers and is a component of a high molecular weight protein complex. *J Biol Chem*
37. Harris HJ, Davis C, Mullins JG, Hu K, Goodall M, Farquhar MJ, Mee CJ, McCaffrey K, Young S, Drummer H, Balfe P, McKeating JA (2010) Claudin association with CD81 defines hepatitis C virus entry. *J Biol Chem* 285:21092–21102
38. Liebner S, Kniesel U, Kalbacher H, Wolburg H (2000) Correlation of tight junction morphology with the expression of tight junction proteins in blood–brain barrier endothelial cells. *Eur J Cell Biol* 79:707–717